Journal of Thermal Science Vol.29, No.2 (2020) 503−511

https://doi.org/10.1007/s11630-020-1225-2 **Article ID: 1003-2169(2020)02-0503-09**

Experimental Investigation of Heat Storage and Heat Transfer Rates during Melting of Nano-Enhanced Phase Change Materials (NePCM) in a Differentially-Heated Rectangular Cavity

LI Zirui[1], HU Nan[1*], TU Jing[1], FAN Liwu[1,2*]

1. Institute of Thermal Science and Power Systems, School of Energy Engineering, Zhejiang University, Hangzhou 310027, China

2. State Key Laboratory of Clean Energy Utilization, Zhejiang University, Hangzhou 310027, China

Abstract: In this work, an experimental study of melting heat transfer of nano-enhanced phase change materials (NePCM) in a differentially-heated rectangular cavity was performed. Two height-to-width aspect ratios of the cavity, i.e., 0.9 and 1.5, were investigated. The model NePCM samples were prepared by dispersing graphene nanoplatelets (GNP) into 1-tetradecanol, having a nominal melting point of 37°C, at loadings up to 3 wt.%. The viscosity was found to have a more than 10-fold increase at the highest loading of GNP. During the melting experiments, the wall superheat at the heating boundary was set to be 10°C or 30°C. It was shown that with increasing the loading of GNP, both the heat storage and heat transfer rates during melting decelerate to some extent, at all geometrical and thermal configurations. This suggested that the use of NePCM in such cavity may not be able to enhance the heat storage rate due to the dramatic growth in viscosity, which deteriorates significantly natural convective heat transfer during melting to overweigh the enhanced heat conduction by only a decent increase in thermal conductivity. This also suggested that the numerically predicted melting accelerations and heat transfer enhancements, as a result of the increased thermal conductivity, in the literature are likely overestimated because the negative effects due to viscosity growth are underestimated.

Keywords: aspect ratio, graphene nanoplatelets, latent heat storage, melting heat transfer, phase change material, rectangular cavity

1. Introduction

Among the three typical forms of thermal energy storage (TES), i.e., sensible, latent and thermochemical heat storage, latent heat storage based on solid-liquid phase change materials (PCM) has been considered for a wide range of applications due to its high heat storage density and narrow temperature variation span upon heat charging/discharging [1]. Typical geometric shapes such as rectangular, cylindrical, and spherical were considered to be the common latent heat storage enclosures [2]. Among the various shapes, melting of PCM in rectangular cavities has received great attention as an representative geometry with applications to metallurgy, TES and thermal management devices [3,4]. Given the same volume and surface area for heat transfer [5], it was

Received: Feb 03, 2019

Corresponding author: HU Nan; FAN Liwu

E-mail: zju_hunan@zju.edu.cn; liwufan@zju.edu.cn

Nomenclature

A	area of heating surface/m^2	Sb	subcooling factor
B	width/mm	Ste	Stefan number
C_p	specific heat capacity/$kJ \cdot kg^{-1} \cdot K^{-1}$	T	temperature/°C
d	distance/mm	t	time/s
Fo	Fourier number	**Greek symbols**	
g	gravitational acceleration/$m \cdot s^{-2}$	β	volumetric expansion coefficient/K^{-1}
Gr	Grashof number	δ	measurement error
H	height/mm	μ	dynamic viscosity/$m \cdot Pa^{-1} \cdot s^{-1}$
h	overall heat transfer coefficient /$W \cdot m^{-2} \cdot K^{-1}$	ρ	density/$kg \cdot m^{-3}$
k	thermal conductivity/$W \cdot m^{-1} \cdot K^{-1}$	τ	elapsed melting time/s
L	latent heat of fusion/$kJ \cdot kg^{-1}$	**Subscripts**	
M	weight/kg	b	copper block
Nu	Nusselt number	c	cooling boundary
Pr	Prandtl number	h	heating boundary
Q	total heat/J	l	liquid phase
q	heat transfer rate/W	m	melting
q''	heat flux/$W \cdot m^{-2}$	s	solid phase

shown that a shorter melting time of the PCM can be achieved in rectangular cavities in comparison to spherical cavities. Melting in a rectangular cavity that is heated from below has been explored [6], where the heat flow is opposite to gravity. In contrast, a differentially-heated rectangular cavity has also been studied as a classic model with a perpendicular configuration between the heat flow and gravity. The study of melting of a pure metal inside a differentially-heated rectangular cavity can be dated back to the late 1980s [7].

The dynamic charging/discharging performance of TES systems is limited by the low thermal conductivity of most common PCM. Hence, two approaches have been developed to enhance heat transfer in TES systems. The traditional approach is to use extended surfaces with high thermal conductivity, e.g., metal fins or foams, to both increase the effective thermal conductivity of the PCM and the overall heat exchange areas of the TES systems [8]. An alternative approach improves the thermal performance of the TES systems by dispersing highly conductive nanoparticles into the PCM, thus forming nano-enhanced PCM (NePCM) [9], which has been studied as an emerging means of heat transfer enhancement [10].

The melting characteristics of NePCM in a rectangular cavity have been studied extensively in the recent literature. Different from the melting process of a pure PCM, the solid-liquid phases of NePCM are usually opaque, so that the conventional visualization method cannot be used for the melting rate and heat transfer analysis of NePCM. Therefore, most of the efforts are based on numerical simulations. For example, using finite volume method, Arasu and Mujumdar [11] presented the numerically predicted melting process of paraffin wax dispersed with Al_2O_3 nanoparticles in a square enclosure that is heated either from the bottom or from one of the lateral walls. Based on the same type of NePCM, the melting in a rectangular channel was investigated by Elbahjaoui et al. [12] under the same finite volume framework, where the enclosure is heated by passing a heat transfer fluid from the outside. Using finite element method, Dhaidan et al. [13] studied numerically the melting of *n*-octadecane suspended with CuO nanoparticles inside a square cavity that is heated from one of the lateral walls at a constant heat flux. More recently, using the lattice Boltzmann method, Feng et al. [14] simulated the melting process of ice, dispersed with copper nanoparticles, in a rectangular cavity that is heated from the bottom. Through analyzing the variations of melting rate and Nusselt number, these numerical studies obtained consistent conclusions that the melting process of NePCM can be accelerated due to the presence of the nano-enhancers, and that the relative improvement becomes more pronounced with increasing the loading of the nanoparticles.

However, as opposed to the findings of the numerical results, the experimental investigation of melting of *n*-octadecane suspended with Al_2O_3 nanoparticles in a differentially-heated square cavity at the lateral walls suggested that the heat transfer during melting is deteriorated markedly with increasing the mass fraction of the nanoparticles [15]. The weakened natural convection in the melted region as a result of the significantly increased viscosity of the NePCM was

deemed to be the primary reason for such heat transfer deterioration. According to the in-house measured thermophysical properties of the NePCM samples [16], it was clear that the negative effect of viscosity growth on melting heat transfer due to the presence of the nanoparticles was underestimated to a great extent by the numerical studies. In this work by Ho and Gao [15], however, the geometric configuration was only limited to a square cavity with a fixed aspect ratio of unity, and the thermal conductivity enhancement of the NePCM based on Al_2O_3 nanoparticles was not that high. Also, the melting heat transfer rate was only evaluated by the average Nusselt number, which was unable to directly reflect the heat storage rate because the latent heat of fusion decreases for the NePCM upon increasing the loading.

Therefore, the experimental study of melting of NePCM in a differentially-heated rectangular cavity can be extended by simply varying the aspect ratio. As a measure of the intensity of natural convection, the Grashof number grows with the third power of the characteristic length so that the effect of natural convection can be easily altered by changing the aspect ratio. In addition, the use of NePCM based on carbon nanomaterials with superior thermal conductivity [17], as compared to the metal oxide nanoparticles, may have a better chance to get enhanced melting and heat storage rates. It was shown that the use of alcohol-based NePCM with dispersing graphene nanoplatelets (GNP) in an isothermally-heated spherical capsule [18] or in a cylindrical container heated from below [19] can lead to enhanced melting heat transfer under certain geometric and thermal configurations and at relatively low GNP contents.

To extend the existing knowledge, the melting of NePCM, dispersed with GNP at various loadings, in a differentially-heated rectangular cavity with two height-to-width aspect ratios was studied experimentally in this work. Also varied was the heating boundary temperature (i.e., the wall superheat). Upon analyzing the melting process in the presence of NePCM, attention was paid to the variations of both heat storage and heat transfer rates.

2. Experimental Details

The two-dimensional physical model of melting of a NePCM in a rectangular cavity (having a height-to-width aspect ratio of H/B) that is differentially-heated at the two opposite lateral walls is shown in Fig. 1(a). In this configuration, the left side wall is heated at a higher temperature T_h, while the opposite wall at the right is maintained at a lower temperature T_c. The bottom and top walls are insulated. The assembly of the melting test rig is schematically shown in Fig. 1(b), which mainly consisted of the melting test section, two constant-temperature water baths, a thermostat chamber and a data acquisition system. The rectangular cavity was mainly made of thick plexiglas boards. While maintaining a constant inner height of the cavity at 25 mm, the inner width was set to be either 25 mm or 15 mm (see Fig. 1(c)). The inner depth along the direction perpendicular to the paper was 60 cm.

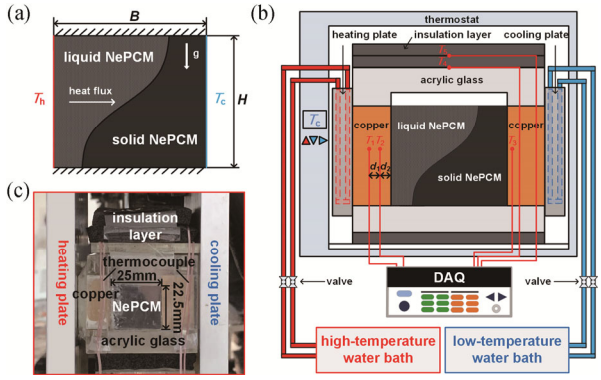

Fig. 1 (a) Physical model for melting of NePCM in a differentially-heated rectangular cavity, (b) schematic diagram of the experimental setup, and (c) photograph showing the assembly of the differentially-heated rectangular cavity (for the case of aspect ratio of 0.9)

The two active walls were made of copper for a better temperature uniformity. Each copper block was attached to an aluminum plate with internal flow channels, followed the setup by Zeng et al. [20]. Each plate was connected to a water bath having a stability of 0.01°C for boundary temperature control. A thin layer of thermal paste was applied to lower the thermal interfacial resistance between the copper block and the aluminum plate. In order to minimize the heat losses, the test section was wrapped by a heavy insulation jacket (only the insulation layer over the top wall is explicitly shown in Fig. 1(c)). Calibrated T-type thermocouples (TCs) with an accuracy of 0.2°C were mounted at different locations, as shown in Fig. 1(b). The two TCs inserted into the left copper block were used to calculate the heat flux transferred through the heating boundary to the NePCM, as proposed by Fan et al. [21], while the cooling boundary temperature was monitored by another TC. The other two TCs were mounted in the top insulation layer to estimate the heat loss through the top wall.

In this work, the NePCM samples were prepared by dispersing graphene nanoplatelets (GNP) into 1-tetradecanol at two loadings of 1 wt.% and 3 wt.% through mechanical agitation and ultrasonic vibration. During the preparation process, it was easily to sense that the NePCM sample becomes more viscous upon

introducing the GNPs and there is a dramatic viscosity growth at the highest loading of 3 wt.%. Prior to each melting run, filling of the empty rectangular cavity was done by slowly pouring a premelted NePCM sample into the cavity. The solidification process was started by controlling the cooling plate at a temperature far below the melting point (37°C). To minimize void formation during the solidification process, a layer-by-layer strategy was adopted in the way that at each step only a small amount of the liquid NePCM sample was added and allowed for a complete solidification of the thin layer.

Moreover, as shown in Fig. 1(b), a 2.5 mm air gap below the lid was reserved to accommodate the volume expansion upon melting. Therefore, the two active walls had an actual height of only 22.5 mm (see Fig. 1(c)). Therefore, the two actual aspect ratios were H/B = 0.9 and 1.5. After formation of the solid NePCM sample in the cavity, the temperatures of the cooling plate and the thermostat were both set at T_c = 37°C for an only 1°C initial subcooling. A uniform initial temperature within the solid NePCM was ensured by maintaining it in the controlled environment for 12 hrs. A melting run was then started by raising the temperature of the heating plate to the desired heating boundary temperature. The heating boundary temperature (T_h) was set at two different values of 47°C or 67°C, i.e., equivalent to a superheat of 10°C or 30°C, respectively. Repetitive experiments up to 3 times were performed for each case to ensure data reproducibility.

3. Data Reduction

Following the work by Fan et al. [21], the melting experimental data were processed. Under the assumption of one-dimensional heat conduction (by ignoring the lateral heat losses), the surface-averaged heat flux q" through the heating plate was determined by

$$q'' = \frac{k_b\left(T_1 - T_2\right)}{d_1} \tag{1}$$

where k_b is the thermal conductivity of the copper block; T_1 and T_2 represent the temperature readings from the two TCs inserted in the heating copper block, and d_1 = 3 mm is the distance between the two TCs (see Fig. 1(b)). The one-dimensional assumption was well justified by the high thermal conductivity of copper and the negligible heat losses through the insulation jacket.

The temperature at the right end of the heating plate (T_h) was then estimated by

$$T_h = T_2 - \frac{q''d_2}{k_b} \tag{2}$$

where d_2 = 2 mm is the distance of the thermocouple from the right end of the heating plate.

The total heat transfer coefficient h involving both conduction and convection during melting of the NePCM was defined by

$$h = \frac{q''}{T_h - T_m} \tag{3}$$

where T_m is the melting temperature of 1-tetradecanol (37°C).

After obtaining the heat transfer coefficient, the average Nusselt (Nu) number was calculated by

$$Nu = \frac{hB}{k} \tag{4}$$

where k is the thermal conductivity of the liquid NePCM.

The maximum heat storage Q_{max} by the NePCM in the rectangular cavity was calculated by

$$Q_{max} = M + \left[L + C_{p,s}\left(T_m - T_c\right) + C_{p,l}\left(\frac{T_h - T_m}{2}\right)\right] \tag{5}$$

where M is the weight of the NePCM.

Furthermore, the instantaneous heat storage of the NePCM over an elapsed time period τ was evaluated by numerical integration of the average heat flux q", which was presented in a dimensionless form

$$Q^* = \frac{A}{Q_{max}}\int_0^\tau q''\mathrm{d}t \tag{6}$$

where A is the heating surface area, and according to data acquisition frequency, the time interval Δt for integration is 1 s.

The Grashof (Gr) number that measures the natural convection intensity during the melting process was defined as

$$Gr = \frac{\rho_l^2 g\beta\left(T_h - T_m\right)B^3}{\mu^2} \tag{7}$$

where ρ_l, β, and μ are the density, volume expansion coefficient, and viscosity of liquid NePCM, respectively, and g is the gravitational acceleration.

The dimensionless time, i.e., the Fourier (Fo) number, was defined as

$$Fo = \frac{kt}{\rho_l C_{p,l} B^2} \tag{8}$$

where $C_{p,l}$ is the specific heat capacity of liquid NePCM.

The Stefan (Ste) number that measures the driving force of melting was defined by

$$Ste = \frac{C_{p,l}\left(T_h - T_m\right)}{L} \tag{9}$$

The Prandtl (Pr) number that quantifies the momentum diffusion (ν) relative to thermal diffusion (α) was defined by

$$Pr = \frac{\nu}{\alpha} \tag{10}$$

Moreover, the subcooling factor (Sb), which measures the ratio of the superheat to subcooling, was defined by

$$Sb = \frac{T_h - T_m}{T_m - T_c} \tag{11}$$

In the calculations, the measured thermophysical properties of the NePCM samples at the temperatures/

phases of interest were described in detail in the work of Fan et al. [21], which are listed in Tab. 1. The uncertainties associated with the data reduction were estimated based on the error propagation theory. For instance, the relative uncertainty for determination of the surface-averaged heat flux, using Eq. (1), was found by

$$\frac{\delta q''}{q''}=\sqrt{\left(\frac{\delta k_b}{k_b}\right)^2+\left[\frac{\delta\left(T_1-T_2\right)}{T_1-T_2}\right]^2+\left(\frac{\delta d_1}{d_1}\right)^2} \tag{12}$$

where the symbol δ in front of a quantity represents its absolute measurement uncertainty. Similarly, the uncertainties for all of the reduced quantities were determined, as given in Tab. 2, which primarily stem from the experimental uncertainties for temperature measurements as well as for determination of the thermophysical properties that were given based upon the spreading of the measured results over parallel tests on multiple specimens.

Table 1 Measured thermophysical properties of the NePCM samples at various mass fractions

Property	Unit	0.0 wt.%	1.0 wt.%	3.0 wt.%
Density ρ_s at 36.5°C	kg/m^3	867.9±1.9	873.4±2.3	884.6±1.2
Density ρ_l at 42°C	kg/m^3	818.8±0.2	823.1±0.2	833.9±0.1
Density ρ_l at 52°C	kg/m^3	809.7±0.1	814.2±0.1	825.2±0.2
Specific heat capacity $C_{p,s}$ at 15–30°C	kJ/(kg·K)	2.04±0.11	1.99±0.08	1.91±0.09
Specific heat capacity $C_{p,l}$ at 45–60°C	kJ/(kg·K)	2.36±0.12	2.30±0.11	2.19±0.10
Thermal conductivity k at 45°C	W/(m·K)	0.159±0.001	0.260±0.001	0.320±0.001
Dynamic viscosity μ at 42°C	mPa·s	13.02±0.04	51.52±0.12	170.06±0.42
Dynamic viscosity μ at 52°C	mPa·s	9.31±0.02	31.98±0.07	139.03±0.26
Latent heat of fusion L	kJ/kg	227.8±3.0	212.2±2.8	183.5±2.4

Table 2 Uncertainties for the measured thermophysical properties and reduced quantities

Property	Uncertainty/%
Density ρ /kg·m^{-3}	0.97
Specific heat capacity C_p /kJ·kg^{-1}·K^{-1}	1.68
Thermal conductivity k /W·m^{-1}·K^{-1}	1.95
Dynamic viscosity μ /mPa·s	5.72
Latent heat of fusion L /kJ·kg^{-1}	0.59
Width of enclosure B /mm	0.13
Average heat flux q" /W·m^{-2}	2.79
Overall heat transfer coefficient h/W·m^{-2}·K^{-1}	2.80
Dimensionless heat storage Q^*	3.96
Nusselt number Nu	3.41
Grashof number Gr	11.7
Fourier number Fo	2.76

The transient variations of the rate of heat transfer into the cavity (through the heating boundary) and the total heat loss from the cavity during melting of pure 1-tetradecanol (i.e., the 0 wt.% NePCM sample) under the lower superheat ΔT = 10°C and in the H/B = 1.5 slender cavity are compared in Fig. 2. As compared to the heat transfer rate between 2.2 W and 8.3 W, the heat loss remains at a low level of only ~0.12 W during the entire course of melting. This is equivalent to a relative heat loss no greater than 5.5%, thus demonstrating the well control of the heat losses in the melting experimental

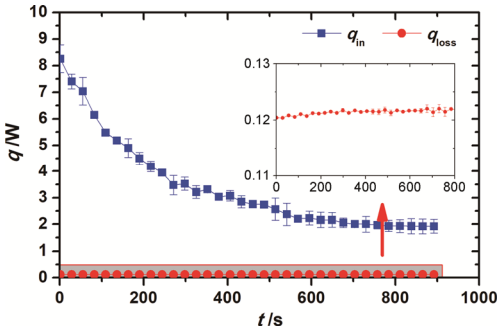

Fig. 2 Instantaneous rate of heat transfer and total heat loss during melting of a pure PCM in a rectangular cavity with the configuration of H/B = 1.5 and ΔT = 10°C

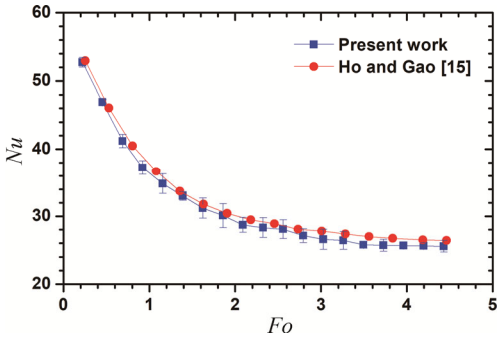

Fig. 3 Comparison of the measured variations of the surface-averaged Nu number during melting of a pure PCM in a rectangular cavity between the present work and the literature (Ho and Gao [15])

setup. In addition, to verify the measured data for melting heat transfer, a special case with an actual aspect ratio of unity (i.e., $H = B = 25$ mm) was tested for the pure PCM. The measured surface-averaged Nu number over the heating boundary as a function of the Fo number is plotted in Fig. 3, which exhibits a very good agreement with the results obtained by Ho and Gao [15] for melting of another pure PCM (*n*-octadecane) in a differentially-heated square cavity having exactly identical inner dimensions.

4. Results and Discussion

4.1 Heat storage rate

The variations of the instantaneous dimensionless heat storage Q^*, as calculated using Eq. (6), for the variety of NePCM samples at the two wall superheats are compared in Fig. 4. As expected, the instantaneous heat storage continues to rise as melting proceeds. For the cavity with an aspect ratio of 0.9, as shown in Fig. 4(a) and 4(c), the NePCM samples with various loadings of GNPs exhibit nearly the same heat storage rate during the initial stage of melting (for $Fo < \sim 1$), regardless of the superheat (i.e., 10°C or 30°C). In either Fig. 4(a) or Fig. 4(c), it is also found that as melting develops the three curves start departing from one another.

The curve for the pure PCM (i.e., the 0 wt.% NePCM) is the fastest to reach unity. There is an inverse relationship between the GNP loading and the dimensionless time for a full charging of the cavity (i.e., when $Q^* = 1$). When there is only a thin melt film along the heating side wall during the initial stage of melting, conduction is the dominant mode of heat transfer and the slightly increased thermal conductivity of the various NePCM samples, as listed in Tab. 1, does not lead to significant changes in the heat storage rate. However, as the melt region expands with the development of melting, the part of contribution from natural convection to the total heat transfer becomes more pronounced. As shown in Tab. 1, the dramatic growth of viscosity of the loaded NePCM samples leads to significantly deteriorated natural convection that overweighs the slightly enhanced heat conduction. As a result of the competition between these two effects, the use of the NePCM samples may slow down the heat storage process.

However, when the width of the cavity was reduced to give rise to a greater aspect ratio of 1.5, as shown in Fig. 4(b) and 4(d), the instantaneous heat storage during the early stage of the melting process exhibits a positive correlation with the loading of GNPs. In either Fig. 4(b) or 4(d), the crossing point among the three curves can be found during the late stage of melting, then a negative correlation is seen approaching the end of melting. According to the definition of the Gr number, the intensity of natural convection varies with the 3rd power

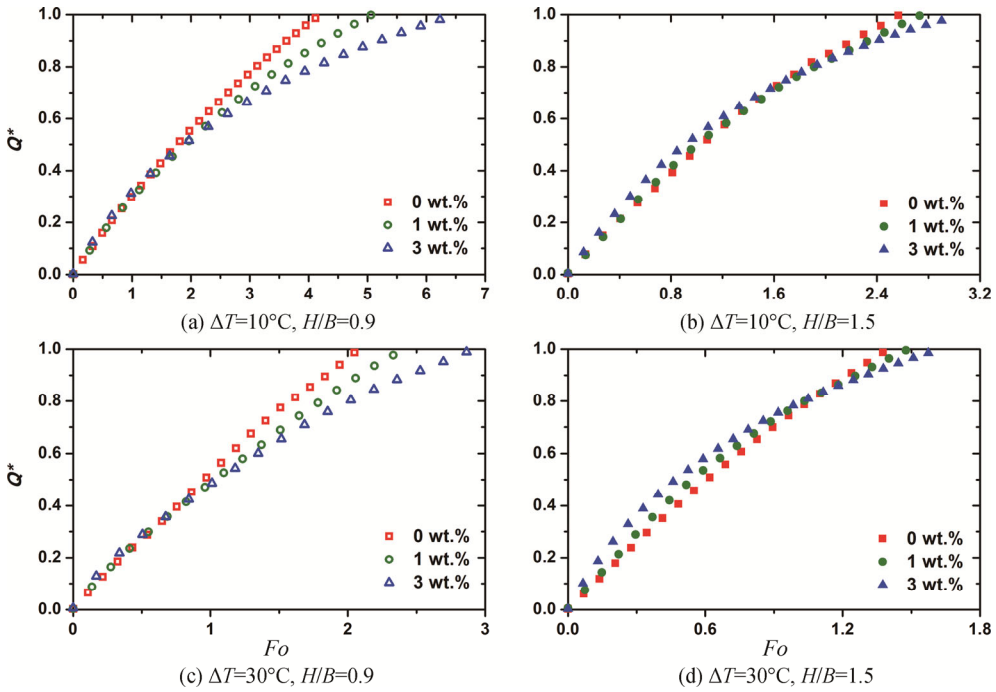

Fig. 4 Variations of the non-dimensional instantaneous heat storage as a function of the Fo number for the various NePCM samples with different geometric and thermal configurations: (a) $\Delta T = 10$°C, $H/B = 0.9$, (b) $\Delta T = 10$°C, $H/B = 1.5$, (c) $\Delta T = 30$°C, $H/B = 0.9$, and (d) $\Delta T = 30$°C, $H/B = 1.5$

Table 3 Grashof number for the NePCM samples under different working conditions

Aspect ratio (H/B)	T_h /°C	0.0 wt.%	1.0 wt.%	3.0 wt.%
0.9	47	4242.79	256.22	23.85
	67	23039.42	1956.55	103.45
1.5	47	961.78	121.36	5.61
	67	5289.15	455.14	28.23

of the characteristic length (i.e., the width of the cavity in this work). The predicted *Gr* numbers for the various cases are listed Tab. 3. Obviously, in this slender cavity with a much narrower gap between the differentially-heated side walls, the relative influence of natural convection is confined to be much weaker. Therefore, the advantage of enhanced heat conduction due to the increased thermal conductivity can be taken to a great extent in this scenario. Similar to the previous experimental studies in other geometries [18,19], the use of NePCM may not be beneficial for accelerated heat storage despite the enhanced thermal conductivity.

4.2 Heat transfer rate

The variations of the surface-averaged *Nu* number over the heating boundary are compared among the various cases in Fig. 5. For all cases, the *Nu* number becomes smaller as melting proceeds, which is similar to the observation in the previous work by Ho and Gao [15]. The *Nu* number for the baseline case of pure PCM is always higher than those of the loaded NePCM samples. In accordance to the decelerated heat storage rate, the heat transfer rate also becomes lower with increasing the loading of the GNPs at any geometric and thermal configurations. This directly confirms that the presence of GNPs, which leads to the significantly increased viscosity that suppresses natural convection, can deteriorate the melting heat transfer. Comparing the melting of a NePCM sample (with the same loading of GNPs) in cavities with different sizes at the same wall superheat (for both ΔT = 10°C and 30°C, as shown in Fig. 5(a) and Fig. 5(b), respectively), it can be found that for all cases the *Nu* number in the nearly square cavity (H/B = 0.9) was significantly higher than that in the more slender one (H/B = 1.5) because natural convection in the cavity with a lower aspect ratio is intrinsically stronger.

Moreover, for the two cavity sizes at the same superheat, reducing the characteristic length of the cavity can effectively shorten the gap between the curves of the loaded NePCM samples and the baseline case of pure PCM. In the slender cavity (H/B = 1.5) where natural convection is relatively weak due to the space confinement effect, the heat transfer can be temporarily

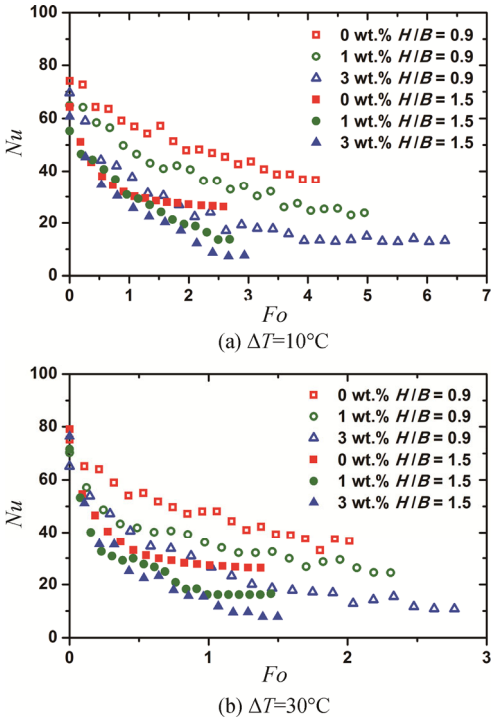

Fig. 5 Variations of the surface-averaged *Nu* number as a function of *Fo* number for the various NePCM samples at the wall superheat of (a) ΔT = 10°C and (b) ΔT = 30°C

enhanced by the loaded NePCM samples during the early stage of melting by taking advantage of the exaggerated positive influence of the increased thermal conductivity.

Having presented the direct comparison of the *Nu* number among the various cases, a scaling analysis was also performed for correlating the variations of the *Nu* number in terms of the combination of dimensionless groupings. As shown in Fig. 6, the correlations were obtained for the *Nu* number by adopting the form suggested by Ho and Gao [15], as given by

$$Nu = \exp\left[X + \frac{Y}{x\left(Gr \cdot Pr\right)^{y}\left(\frac{Ste \cdot Fo}{1+Sb}\right)^{z} + Z}\right] \tag{13}$$

where the index x, y, z and coefficient X, Y, Z are constants to be determined.

As shown in Fig. 6, all the measured *Nu* number data were collected together for a specific NePCM sample. The constants in Eq. (13) were determined by means of curve fitting, as listed in Tab. 4. These correlations may be used for predicting the melting heat transfer of the NePCM samples in a differentially-heated rectangular cavity with the various geometric and thermal configurations with an acceptable accuracy.

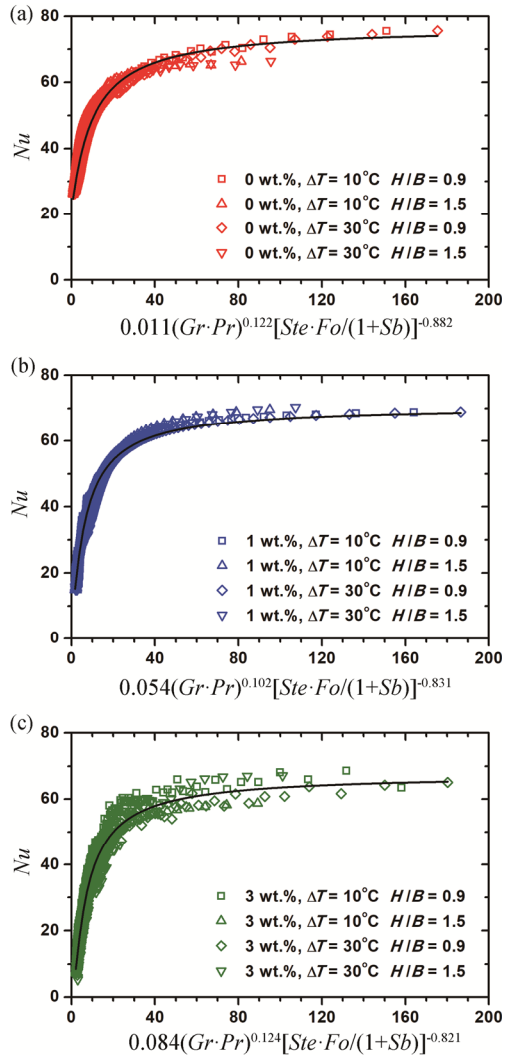

Fig. 6 Variations of surface-averaged *Nu* number as correlated to a specific combination of dimensionless groupings for the (a) 0 wt.%, (b) 1 wt.%, and (c) 3 wt.% NePCM samples

Table 4 Constants as determined by curve fitting of the correlation, Eq. (13), of the averaged Nusselt number.

φ/ wt.%	x	y	z	X	Y	Z	R^2
0.0	0.011	0.122	−0.882	4.344	−7.062	5.509	0.93
1.0	0.054	0.102	−0.831	4.260	−5.891	2.117	0.96
3.0	0.084	0.124	−0.821	4.214	−6.375	1.028	0.94

5. Conclusions

In this work, an experimental study of the melting heat transfer of GNP-based NePCM in a differentially-heated rectangular cavity was carried out. The instantaneous variations of the dimensionless heat storage and the *Nu* number during melting were measured for the various combinations of two rectangular cavity sizes, two heating boundary temperatures and three loadings of GNPs. It was found that the overall heat storage and heat transfer rates of pure PCM are higher than those of the loaded NePCM samples, and that there is a monotonous deterioration of melting with increasing the GNP loading. Although a decent increase in thermal conductivity can be achieved for the NePCM samples, the dramatic viscosity growth that deteriorates significantly natural convection heat transfer can overweigh the enhanced heat conduction.

Moreover, reducing the characteristic length of the cavity can take more advantage of the increased thermal conductivity of NePCM because the natural convection effect in a smaller cavity is intrinsically weaker due to the space confinement. In other words, this leads to a relatively increased contribution of heat conduction to the overall melting heat transfer process, thus mitigating the negative effect due to viscosity growth. Based on the specific NePCM samples studied, the experimental results suggested that the numerical predictions in the literature that claim melting acceleration and heat transfer enhancement as a result of the increased thermal conductivity may not be true in the realistic cases for NePCM with a remarkable increase in viscosity, because the significantly suppressed natural convection effect is likely underestimated by the numerical predictions.

Acknowledgments

This material is based upon work supported by the Zhejiang Provincial Natural Science Foundation of China under Grant No. LR17E060001. FAN Liwu would like to thank a start-up fund granted by the "100 Talents Program" of Zhejiang University.

References

[1] Zalba B., Marín J.M., Cabeza L.F., Mehling H., Review on thermal energy storage with phase change: materials, heat transfer analysis and applications. Applied Thermal Engineering, 2003, 23(3): 251–283.

[2] Fukusako S., Yamada M., Melting heat transfer inside ducts and over external bodies. Experimental Thermal and Fluid Science, 1999, 19(2): 93–117.

[3] Dhaidan N.S., Khodadadi J.M., Melting and convection of phase change materials in different shape containers: A review. Renewable and Sustainable Energy Reviews, 2015, 43: 449–477.

[4] Krishna J., Kishore P.S., Solomon A.B., Heat pipe with nano enhanced-PCM for electronic cooling application. Experimental Thermal and Fluid Science, 2017, 81: 84–92.

[5] Vyshak N.R., Jilani G., Numerical analysis of latent heat

thermal energy storage system. Energy Conversion and Management, 2007, 48(7): 2161–2168.

[6] Zhou J., Chen Z., Liu D., Li J., Experimental study on melting in a rectangular enclosure heated below with discrete heat sources. Journal of Thermal Science, 2001, 10(3): 254–259.

[7] Beckermann C., Viskanta R., Effect of solid subcooling on natural convection melting of a pure metal. ASME Journal of Heat Transfer, 1989, 111(2): 416–424.

[8] Fan L.W., Khodadadi J.M., Thermal conductivity enhancement of phase change materials for thermal energy storage: A review. Renewable and Sustainable Energy Reviews, 2011 15(1): 24–46.

[9] Khodadadi J.M., Fan L.W., Babaei H., Thermal conductivity enhancement of nanostructure-based colloidal suspensions utilized as phase change materials for thermal energy storage: a review. Renewable and Sustainable Energy Reviews, 2013, 24: 418–444.

[10] Rao S.S., Srivastava A., Whole field measurements to understand the effect of nanoparticle concentration on heat transfer rates in a differentially-heated fluid layer. Experimental Thermal and Fluid Science, 2018, 92: 326–345.

[11] Arasu A.V., Mujumdar A.S., Numerical study on melting of paraffin wax with Al_2O_3 in a square enclosure. International Communications in Heat and Mass Transfer, 2012, 39(1): 8–16.

[12] Elbahjaoui R., El Qarnia H., El Ganaoui M., Melting of nanoparticle-enhanced phase change material inside an enclosure heated by laminar heat transfer fluid flow. The European Physical Journal Applied Physics, 2016, 74(2): 24616.

[13] Dhaidan N.S., Khodadadi J.M., Al-Hattab T.A., Al-Mashat S.M., Experimental and numerical investigation of melting of phase change material/ nanoparticle suspensions in a square container subjected to a constant heat flux. International Journal of Heat and Mass Transfer, 2013, 66: 672–683.

[14] Feng Y., Li H., Li L., Bu L., Wang T., Numerical investigation on the melting of nanoparticle-enhanced phase change materials (NEPCM) in a bottom-heated rectangular cavity using lattice Boltzmann method. International Journal of Heat and Mass Transfer, 2015, 81: 415–425.

[15] Ho C.J., Gao J.Y., An experimental study on melting heat transfer of paraffin dispersed with Al_2O_3 nanoparticles in a vertical enclosure. International Journal of Heat and Mass Transfer, 2013, 62: 2–8.

[16] Ho C.J., Gao J.Y., Preparation and thermophysical properties of nanoparticle-in-paraffin emulsion as phase change material. International Communications in Heat and Mass Transfer, 2009, 36(5): 467–470.

[17] Yu Z.T., Fang X., Fan L.W., Wang X., Xiao Y. Q., Zeng Y., Increased thermal conductivity of liquid paraffin-based suspensions in the presence of carbon nano-additives of various sizes and shapes. Carbon, 2013, 53: 277–285.

[18] Fan L.W., Zhu Z.Q., Zeng Y., Ding Q., Liu M.J., Unconstrained melting heat transfer in a spherical container revisited in the presence of nano-enhanced phase change materials (NePCM). International Journal of Heat and Mass Transfer, 2016, 95: 1057–1069.

[19] Hu N., Zhu Z.Q., Li Z.R., Tu J., Fan L.W., Close-contact melting heat transfer on a heated horizontal plate: revisited in the presence of nano-enhanced phase change materials (NePCM). International Journal of Heat and Mass Transfer, 2018, 124: 794–799.

[20] Zeng Y., Fan L.W., Xiao Y.Q., Yu Z.T., Cen K.F., An experimental investigation of melting of nanoparticle-enhanced phase change materials (NePCMs) in a bottom-heated vertical cylindrical cavity. International Journal of Heat and Mass Transfer, 2013, 66: 111–117.

[21] Fan L.W., Zhu Z.Q., Zeng Y., Lu Q., Yu Z.T., Heat transfer during melting of graphene-based composite phase change materials heated from below. International Journal of Heat and Mass Transfer, 2014, 79: 94–104.